Modulation of Low-latitude West Wind on Abnormal Track and Intensity of Tropical Cyclone Nargis (2008) in the Bay of Bengal

Wei-Wei Li [1], Chunzai Wang [2], Dongxiao Wang [1], Lei Yang [1], Yi Deng [1]

[1] Key Laboratory of Tropical Marine Environmental Dynamics, South China Sea Institute of Oceanology, Chinese Academy of Sciences, P R China

[2] NOAA/Atlantic Oceanographic and Meteorological Laboratory, Miami, Florida, USA.

(Received 27 December 2010, revised 14 July 2011)

Corresponding author:

Dr. Dongxiao Wang

Key Laboratory of Tropical Marine Environmental Dynamics

South China Sea Institute of Oceanology, Chinese Academy of Sciences

164 West Xingang Road, Guangzhou 510301, China

Phone: (86)20-8902-3204; Fax: (86)20-8902-3205

E-mail: dxwang@scsio.ac.cn

Abstract

Tropical cyclone (TC) Nargis made landfall in Myanmar on 02 May 2008, bringing a storm surge, major flooding, and resulting in a significant death toll. TC Nargis displayed abnormal features, including rare eastward motion in its late stage, rapid intensification before landing, and etc. Using reanalysis data and a numerical model, we investigated how a low-latitude westerly wind modulated TC Nargis' track and provided favorable atmospheric conditions for its rapid intensification. More importantly, we found a possible counterbalance effect of flows from the two hemispheres on the TC track in the Bay of Bengal. Our analysis indicates that a strong westerly wind burst across the Bay of Bengal, resulting in TC Nargis' eastward movement after its recurvature. This sudden enhancement of westerly wind was mainly due to the rapidly intensified mid-level cross-equatorial flow. Our results show that a high-pressure system in the Southern Hemisphere induced this strong, mid-level, cross-equatorial flow. During the rapid intensification period of TC Nargis, this strong and broad westerly wind also transported a large amount of water vapor to TC Nargis. Sufficient water vapor gave rise to continuously high and increased mid-level relative humidity, which was favorable to TC Nargis' intensification. Condensation of water vapor increased the energy supply, which eventuated the intensification of TC Nargis to a category 4 on the Saffir-Simpson scale.

Keywords: TC Nargis, tropical cyclone, westerly wind, cross-equatorial flow, Bay of Bengal.

Doi: 10.1007/s00376-011-0229-y.

1. Introduction

The Indian subcontinent is one areas in the world affected most severely by tropical cyclones (TCs), although TCs in this region account for ~7% of the total number of global TCs (Gray, 1968). Unlike TCs in the Western Pacific that mainly occur after the monsoon onset, TCs in the Bay of Bengal (BOB) have two seasons. The primary season is the post-monsoon period and the second is the pre-monsoon season (Mohanty, 1994). During the monsoon, less TCs or tropical disturbances occur because strong tropospheric ventilation produced by the large vertical wind shear inhibits storm development (Gray, 1968). Compared with TCs in the Pacific and hurricanes in the Atlantic (e.g., Liu et al., 2010; Li et al., 2011; Yuan et al., 2009), the TC genesis process in the northern Indian Ocean has received little attention, probably because of a lack of observation data. Kikuchi et al. (2009) indicated that incipient disturbances were virtually absent in the northern Indian Ocean and that the initiation process of tropical depression was expected to be different from those in the Pacific and Atlantic Oceans.

TC tracks in the BOB can be classified as westward, north-to-northwestward, and eastward. The westward and north-to-northwestward tracks are dominant, whereas an eastward track is relatively rare. Some TCs with severe intensity initially move northwestward and then turn eastward or northeastward (IMD, 1996; Rao, 1997). TC Nargis (2008) was a TC of this type. The TC track is affected by many internal and external factors (Mohanty et al., 1997). Steering flow is the prominent external force on TCs, accounting for 70–90% of a TC's motion (Chan, 2005). When the steering

flow is weak, TCs tend to move poleward and westward as a result of internal force (Chan et al., 1982; Elsberry et al., 1987). In addition, TCs tend to move toward a warmer ocean surface (Orlanski, 1998; Mandal et al., 2007). In recent years, some progress has been made using models for operational TC track forecasting in India (Mohanty et al., 1997; Gupta et al., 1997; Prasad et al., 2003). Nevertheless, little has been done to investigate physical factors controlling the TC track in the Indian Ocean. The purpose of the present study was to address this issue by focusing on the physical factors controlling the TC track of TC Nargis.

TC Nargis, which caused a large number of fatalities, formed and developed in late April 2008. After its recurvature, it reached category 4 on the Saffir-Simpson scale, then it made a landfall in Myanmar on 02 May (e.g., Webster, 2008; Lin et al., 2009). Since then studies have been performed that have examined different aspects of the TC. The relationship between TC Nargis' initiation and the Madden-Julian Oscillation (MJO) has been discussed by Kikuchi et al. (2009) and Yanase et al. (2010). They suggested that Nargis was initiated from a Rossby wave vortex that emanated from an abnormally strong intraseasonal westerly event associated with the MJO in the eastern Indian Ocean. Yokoi et al. (2010) concluded that a lower-tropospheric easterly surge associated with a cold surge off the eastern coastal of Eurasian continent triggered the genesis of TC Nargis. The horizontal convergence at the head of the surge associated with active convection was considered as an external forced convergence that triggered its genesis. Shen et al. (2010), using a global mesoscale model to predict TC genesis, found that a westerly wind burst, an

equatorial trough, an enhanced anti-cyclonic vertical wind shear, and low-level moisture convergence were the key factors in TC Nargis' genesis. Yamada et al. (2010) found that the meander of the mid-tropospheric dry flow and the structural change to be related to the abnormal track of TC Nargis. They attributed this flow to the subsidence along the south margin of Tibetan Plateau. In terms of air–sea interaction, the ocean responses such as temperature and salinity were analyzed using real-time mooring and satellite data (McPhaden et al., 2009). Emanuel (1999) indicated that the heat exchange with the upper layer of the ocean under the core of the hurricane was one of the factors that determined the evolution of the TC's intensity. Based on this theory, Lin et al. (2009) found that TC Nargis' rapid intensification (RI) took place on a pre-existing warm ocean anomaly in the BOB that increased the air-sea enthalpy flux to support RI.

These previous studies regarding TC Nargis mainly focused on its genesis and the effect of air–sea interaction on RI. As mentioned above, Yamada et al. (2010) attributed TC Nargis' recurvature to the mid-tropospheric dry flow. However, the contribution of other controlling factors' to TC Nargis' unique track remains unknown. The source of significant westerly wind across the BOB should not be the only mid-tropospheric dry flow from the south margin of Tibetan Plateau (Yamada et al., 2010), especially in the late stage. Moreover, TC Nargis was unique but not unprecedented. The similar TCs in April and May have occurred before and will form in the future. Clarifying the physical background of a storm like TC Nargis will help to minimize the error of operational forecasting for similar TCs in the future, and

perhaps even reduce the loss of lives and property.

Therefore, the focal point of the present study was to explain how a low-latitude westerly wind modulated TC Nargis' track and provided favorable atmospheric conditions for its RI. In addition, we investigated the mechanism of the sudden enhancement of low-latitude westerly wind. From the simulation, we were able to test the ability of the model to simulate TC Nargis' track. Based on this simulation, we conducted a sensitivity experiment in which the relative humidity (RH) was decreased to investigate the impact of RH on TC Nargis' RI. The paper is organized as follows. Datasets used in this study are discussed in Section 2. Modulation of low-latitude westerly wind on the TC track is described in Section 3. Section 4 shows contribution of low-latitude westerly wind to RI, including analysis of environmental RH, water vapor transportation, and latent heat flux. Numerical simulation of TC Nargis' track and other controlling factors by the Weather Research and Forecasting (WRF) model are discussed in Section 5.

2. Data

In this investigation, several datasets were used:

· Historical record of TC activity in the BOB from January 1977 to December 2008 (i.e., the data are more reliable after the 1970s) was obtained from the best-track archives of the Joint Typhoon Warning Center (JTWC). The real-time TC Nargis track data were derived from the Indian National Center for Ocean Information Services (INCOIS), which recorded TC Nargis' center and intensity from 23 April 2008 (McPhaden et al., 2009). We used JTWC data for statistical analysis and

INCOIS for the evaluation of TC Nargis.

- Atmosphere reanalysis data are from two datasets: The NCEP/NCAR Reanalysis 1 project (2.5° resolution) and the NCEP FNL (Final) Operational Global Analysis data (http://dss.ucar.edu/datasets) (1.0° × 1.0° grid, at continuous 6-h intervals) from the Global Forecast System (GFS) at NCEP. The NCEP/NCAR I and II and FNL datasets do not insert "bogus observations." Without adding bogus observations, the storm is weaker and larger compared with the observed storms, and the center is located away from the real storm center. Nevertheless, in this study, investigations were focused on environmental conditions (≥200 km away from the TC center), and the addition of bogus observations would not have impacted the result significantly.
- Daily 1° gridded global surface latent heat flux was obtained from the Objectively Analyzed air–sea heat Fluxes (OAFlux) project. This project develops enhanced air–sea heat flux analysis products for the global oceans. The product integrates satellite observations with surface moorings, ship reports, and atmospheric model reanalyzed surface meteorology (http://oaflux.whoi.edu/heatflux.html).

3. Modulation of low-latitude westerly wind on TC Nargis' track

3.1 Description of track abnormality

TC Nargis formed and developed during late April to early May 2008, during the first frequently occurring period of TCs of the year in the BOB. In this early season, TCs tend to march poleward and then make landfall on the northern coast of the BOB. However, TC Nargis, with an eastward track after the recurvature, made landfall at

Myanmar. Its track was rare in comparison with TC track types from 1977 to 2008 in the BOB (Table 1 and Fig. 1). TCs that form during April and May in the BOB have a greater probability of making landfall to the east than TC of other seasons. These sudden eastward TCs are prone to become powerful and disastrous and to impact the surrounding countries whose populations are dense. In this study, we only discuss the abnormality of its track after TC Nargis' recurvature, as the easterly surge theory from Yokoi et al. (2010) has investigated TC Nargis' development in its earlier stage.

3.2. Steering flow

Under the barotropic atmospheric approximation, a TC is a rotating cylinder embedded in an atmospheric flow of much larger horizontal dimensions, and may therefore be treated as a solid object "floating" in the atmosphere so that its motion is governed by its surrounding flow (Chan, 2005). This is generally referred to as the "steering" concept, and the flow is called the steering flow. In general, the flow at different heights in the atmosphere can be different. Hence, to overcome this problem, an integrated flow (through a deep layer of the atmosphere) is usually considered, which also reduces the dynamics to barotropic (Elsberry, 1987). Hence, the TC vortex (which is baroclinic) was excluded. Velden and Leslie (1991) found that the integration through a deep layer of the atmosphere gives a flow that is closest to the TC motion.

To describe the abnormal feature of TC Nargis' track, we calculated the vertical integrated mass-weighted deep-layer mean velocity as the steering flow (Liu et al., 1998; Weber, 2001): $V_m = \int_{1000hPa}^{300hPa} V_r dp$. The principle of this method is to remove the

effect of vortex and examine the barotropic component of the atmospheric flow (Figs. 2a–b).

Figure 2a–b shows the mass-weighted deep-layer mean and anomaly wind velocity and U-wind fields (i.e., anomaly with the climatology of the same day during 1977–2008), respectively. After recurvature (0000 UTC 29 April), significant eastward barotropic flow appeared across most parts of the BOB. Anomaly fields indicate that northwest wind anomalies spread over the entire BOB. The northerly wind component was partly related to the meander of the mid-tropospheric flow over southern Tibet (Yamada et al., 2010). In terms of the westerly wind component, we considered the contributions of flows derived from both the Northern and Southern Hemispheres (NH and SH).

3.3. Mid-level Cross-equatorial flow intensification

Wind fields at 500 hPa (Fig. 3) were analyzed throughout the main life cycle of TC Nargis (25 April – 2 May), because flow at this level is an effective parameter to interpret the steering flow in the general status of the TC. It shows that, from 27 to 29 April, cold air from the North Arabian Sea invaded southward to the equator and contributed to the westerly wind in the BOB. During this period, the westerly wind gently blew from the southern BOB to the Andaman Sea and arrived in Myanmar on 28 April. This cold air also restricted the inclination of the warm and moist southerly flow around the equator to move northward and intensify. On 30 April, cold air subsided while a significant anticyclonic circulation built up in the SH. This anticyclonic circulation was accompanied by a strong and broad cross-equatorial

northerly flow (CEF, located to the south of India). The β-effect gradually turned the northerly CEF into a westerly wind in the BOB. This significant CEF-induced westerly wind lasted for 3 days until TC Nargis made landfall on 02 May. During this period, TC Nargis underwent a relatively straight eastward movement and in the end assailed the southern part of Myanmar, which is a rare occurrence.

Figure 4 depicts the vertical time section of the CEF wind profile as well as the meridional component of wind (V-wind). The rectangular region shown in Fig. 3 (2.5°S–2.5°N, 70–80°E) was selected for evaluating the evolution of the CEF. It shows that the CEF had already appeared at mid-level since 26 April, but it was weak mainly due to the cold southward air mentioned above (see Fig. 3). From 29 April, a significant mid-level (600–300 hPa) southerly wind began to appear. Strong southerly winda spread from 500 hPa to 300 hPa, which contributed to the strong and broad westerly wind in the BOB, steering TC Nargis to the east.

3.4 Southern hemisphere high pressure system development

Generally, the CEF corresponds to a high pressure system (HPS) or cold air activities in the SH (Simpson, 1921). Geopotential height and wind anomaly field at 500 hPa (i.e., anomaly with the climatology of the same day during 1977–2008) can reveal the atmospheric circulation abnormality and the activities of synoptic scale weather systems. Figure 5 shows that an HPS in the southern Indian Ocean of the SH began to develop after TC Nargis' recurvature. During the next 2 days (30 April and 01 May), two controlling factors resulted in the intensification of the mid-level CEF as well as the appearance of strong and broad westerly wind in the BOB. One controlling factor

was the subsidence of southward cold air, which has already been discussed in section 3.3. This cold air from the North Arabian Sea subsided on 30 April, permitting the mid-level flow south of the equator to cross the equator northward. The other factor was the intensification of the HPS in the SH. A powerful flow from the eastern quadrant of this HPS uniformly moved northward and dominated most of the southern Indian Ocean. This flow finally blew toward Myanmar and steered TC Nargis eastward. In fact, in this TC case, if these two factors had come into balance, the mid-level CEF and westerly wind in the BOB would have been weak. The southward cold airstream would then have been the only source of westerly wind across the BOB, as occurred on 27–28 April and 02 May. On the other hand, if neither of these two factors had converged, TC Nargis probably would not have had an eastward movement.

4. Contribution of CEF-induced westerly wind to TC Nargis' RI

TC Nargis underwent a rapid intensification (RI) period from 06Z 1 May to 06Z 2 May. It intensified from a category 1 to a category 4 TC prior to landfall; the wind increased by 45 knots in 24 h. As Lin et al. (2009) have studied warm sea surface temperature (SST) anomaly effect, in this study we mainly focused on the favorable atmospheric effect on TC Nargis' RI. Results from section 3 demonstrate that the CEF-induced westerly wind across the BOB assisted TC Nargis to move eastward in its late stage. The RI occurred on 01 May when TC Nargis was most affected by this CEF-induced westerly wind (see Figs. 3–4). During the RI period, this westerly wind actually transported a large amount of warm and moist air from the equatorial region

to TC Nargis.

4.1 Favorable environmental relative humidity

Environmental RH has significant effects on the development of TCs (Emanuel, 2003). In this study, we analyzed RHs by area mean (200 km ≤ r ≤ 800 km of the center of TC Nargis) then average between 850 hPa and 700 hPa, as has been done in other model studies (Kaplan et al., 2003; Erb, 2006). A rectangular area (800 km ≤ r ≤ 1000 km of the TC Nargis center to the south) was selected for comparison, as lower latitude is generally warmer and moister than north.

The time series of TC Nargis intensity and RHs is shown in Fig. 6. During the RI period, the mid-level RH of TC Nargis continued to increase and showed a similar value with the selected southern region. The mid-level RHs in both regions were >65% during the RI period, which was favorable to TC development and intensification (Emanuel, 2003). Before 1500 UTC 01 May, TC Nargis' peripheral moisture value was even higher than the southern region. More water vapor was transported to TC Nargis. Nevertheless, it is noteworthy that an RH decrease occurred over the southern region during RI. This possibly occurred because more water vapor was absorbed by the more powerful TC Nargis in this period, although this is not a concern of our study.

4.2 Water vapor transportation by CEF-induced westerly wind

The continuing increased RH suggests that water vapor transport was increasing continuously. Figure 7 shows the accumulated vertical integrated water vapor transport from surface to 300 hPa over the pre-RI period (29–30 April) and the RI

period (1–2 May). Clearly, over TC Nargis' main region, more water vapor was transported from tropics during the RI period than the pre-RI period. In addition, the main water vapor source changed from the South Arabian Sea into the Indian Ocean of the SH. This is consistent with the explanation about the development of mid-level CEF and the HPS in section 3. The water vapor transport during these two periods also accords with the atmospheric circulation shown in Figs. 3–5. Thus, the CEF-induced westerly wind indeed transported a large amount of warm and moist air from equatorial region to TC Nargis, which gave rise to a RH increase during the RI period.

We also examined the possible reason for latent heat flux (LHF) increase during RI period, as LHF is associated with evaporation or transpiration of water and subsequent condensation of water vapor in the troposphere (Perrot, 1998). Figure 8a1–a2 illustrates that the latent heat exchange around TC Nargis increased during RI (01 May to 02 May). The amplification of LHF over TC Nargis' main region exceeded 60 W m^{-2} (Fig. 8b). Admittedly, LHF is also related to sea surface temperature, wind speed, and etc. In addition, Lin et al. (2009) have studied the warm SST anomaly effect on TC Nargis' RI, and the stronger low-level wind of the more powerful TC Nargis would force more latent heat to be released, which in turn intensified TC Nargis by supplying energy. Nevertheless, if sufficient water vapor was provided through this process, condensation of water vapor would help increase the energy supply, leading to an intensification of TC Nargis to a category 4 on the Saffir-Simpson scale. In other words, water vapor brought by the CEF-induced

westerly wind was a necessary factor in TC Nargis' RI.

5. Numerical simulation of TC Nargis

In this part of the study, numerical modeling was supplemented because of the temporal and spatial limitations of observation and reanalysis data. The reproduced physical processes of TC Nargis with numerical models promotes better understanding of the effects of the CEF-induced westerly wind on TC Nargis' track as well as the RH effects on TC Nargis' RI.

Because we were only concerned with the modulation of large-scale atmospheric circulation on TC Nargis' track and the intensity there, we only adopted one domain on Mercator map projections (Fig. 9). The horizontal resolution, grid number, and other physical schemes are presented in Table 2. Simulation was initialized at 1200 UTC 27 April before TC Nargis' recurvature. The integration was carried out for 126 h. Simulation was terminated at 1800 UTC 02 May.

5.1 Simulated track and west wind across BOB

Comparison between the observed track from INCOIS and the simulated track is shown in Fig. 10. In the simulation, TC Nargis turned more northward from 0600 UTC 1 May and began to turn slightly southward 12 h later. The simulated TC Nargis moved a little faster than the observed storm. Although the simulated track differs somewhat from the observation, the general comparison of their trends is favorable, especially the landfall position.

Based on the reasonably well-simulated track, the simulated evolution of wind fields at low-mid level (Eta-7 and Eta-12 level, which are close to 850 hPa and 500

hPa, respectively) were analyzed (Fig. 11). Compared with the steering flow and wind fields derived from the reanalysis data (Figs. 2-3), the simulation reproduced well the cold southward air in the earlier TC stage, the significant CEF from 1200 UTC 28 April, and the broad and strong westerly wind in the BOB (Fig. 11).

5.2 Nargis' sensitivity to CEF-induced wind and RH

Compared with the water vapor transport based on reanalysis data (Fig. 7), the simulation by control experiment also shows that high RH (≥40%) spread across the BOB. Specifically, from the southeast quadrant of TC Nargis, a southwest–northeast water vapor transport channel appeared from 1200 UTC 28 April to 1200 UTC 02 May, which covered the RI period (Fig. 12).

The fact that the simulation successfully reproduced the CEF and the associated westerly wind across the BOB lays a good foundation for the investigation of the impact of the CEF-induced wind as well as the transport of a large amount of warm and moist air on TC Nargis' track and intensity. Based on the above simulation, two numerical sensitivity experiments in which the wind speed and the RH decreased by 50% during the RI period were performed, respectively. The region for the two variables was selected where TC Nargis was mainly affected by the CEF-induced westerly wind (the rectangular region marked in Fig. 9). To isolate the effect of wind, only the wind speed was changed in the sensitivity experiment, and all the other settings remain unchanged in the model. The sensitivity experiment about the RH decrease was conducted using the same method.

Figure 13a–b shows the changes of TC Nargis' track after the CEF-induced wind

weakened and the RH decreased at all levels by 50%. This figure shows that TC Nargis tended to move northward significantly when the CEF-induced wind weakened. On the other hand, TC Nargis' track changed slightly when the RH decreased. This result suggests that the CEF-induced wind contributed more to TC Nargis' track than did the corresponding RH.

To further examine the sensitivity of TC Nargis' intensity to the CEF-induced wind and the environmental RH, we first calculated the difference of the RH between control and sensitive experiments (i.e., the RH from control experiment minus the one from sensitive experiment) with wind speed decreased by 50% at all levels (Fig. 12). Our results show that TC Nargis' environmental RH decreased by >10%, especially in its eastern quadrant. This means that the CEF-induced wind not only affected TC Nargis' movement but also significantly decreased the environmental RH. We also studied the sensitivity of TC Nargis' intensity to the CEF-induced wind (Fig. 14a). Our results show that although the general intensities of both experiments are much weaker than that of the observation (mostly because no nesting was added), a remarkable increase in the minimum central pressure (>10 hPa) appeared when the wind weakened by 50%. Although the decrease of TC Nargis' intensity is also related to the track change [i.e., away from the warm ocean zone (Lin et al. 2009)], the track change essentially resulted from the CEF-induced wind decrease. Therefore, TC Nargis' intensity and environmental RH during RI was sensitive to the CEF-induced wind.

Because the CEF-induced wind significantly affected the environmental RH, we

also studied the contribution of the RH to TC Nargis' intensity. We conducted another numerical sensitivity experiment with the RH decreased by 50%. Figure 14(b) depicts the comparison between the simulated intensity of TC Nargis by control run and that of the numerical sensitivity experiment. It shows that a remarkable increase of the minimum central pressure appeared (>10 hPa) after decreasing the RH at all levels. This result proves that the sensitivity of TC Nargis' intensity to the RH is also significant, which is in accord with the hypothesis of section 4.

The results above suggest that the CEF-induced westerly wind significantly affected TC Nargis' track and intensity. Additionally, the corresponding RH also helped TC Nargis develop and intensify during the RI period, and it was also significantly affected by the CEF-induced wind.

6. Summary and discussion

The schematic of the controlling factors regarding TC Nargis' track and RI is summarized in Fig. 15; it lists factors affecting TC Nargis' unique track and RI in this study. They are the HPS in the SH, the associated mid-level cross-equatorial flow (CEF), and the southward cold air from the northern Arabian Sea. Our results indicate that if the HPS and southward cold air had come into balance, mid-level CEF would have become weak. The southward cold air would have been the only source of westerly wind across the BOB. If neither of these two factors had been present, TC Nargis probably would not have moved eastward in its late stage. On the other hand, the CEF-induced westerly wind at low latitude also provided favorable RH during rapid intensification (RI) period by transporting a large amount of water vapor to TC

Nargis. This helps explain TC Nargis' RI, because high RH is necessary for the development and intensification of a TC. Moreover, condensation of water vapor would increase the latent heat supply for TC Nargis and upgrade its intensification. Numerical modeling and the sensitivity experiment with the decreased wind speed and RH reasonably explained the effects of CEF-induced westerly wind on TC Nargis' track as well as the RH effects on TC Nargis' RI.

This study is of value because of two findings: First, we found a possible counterbalancing effect of flows from the two hemispheres on the TC track in the Bay of Bengal (BOB). We have provided a case of evidence for TC track investigation and forecasting in the BOB future. Moreover, compared with westward and northward TCs, the reason that eastward TCs in the BOB are prone to undergo RI (e.g., TC Nargis (2008), TC Mala (2006), TC 02B (2002), and etc.) can be explored in terms of CEF-induced warm and moist air invasion. Next, we focused our research on the abnormal eastward track of TC Nargis because a TC with this track type directly assaults the communities in the Irrawaddy Delta, which is the lowest expanse of land in Myanmar. Clarifying the physical background of track like TC Nargis' will help to minimize the error of operational forecasting for similar TCs in the future, which will perhaps reduce the loss of lives and property.

Finally, the mid-level CEF intensification in this case needs further discussion. Figure 16 gives the evolution of subtropical westerly jet (SWJ) after TC Nargis' recurvature (from 29 April to 1 May). Clearly, the SWJ became weak. The waning of the SWJ benefits the monsoon transition from the winter to summer pattern. Then the

low-latitude westerly wind or the southwesterly monsoon shifts northward. Such an indirect relationship needs quantization analysis and simulation to substantiate it. Additionally, the relationship between TCs in the BOB and the monsoon onset also needs to be investigated. In fact, TC Nargis ended on 03 May, and the date of monsoon onset in the BOB in 2008 was 10 May, which was 5 days ahead of schedule (as stated by the India Meteorological Department). Therefore it is possible that TC Nargis helped trigger monsoon onset in the BOB. Not only were TCs nurtured by the monsoon but also TC Nargis and similar TCs may have affected monsoon activity. Whether there exists a feedback-like mechanism between TCs and the monsoon deserves study in the future.

Acknowledgements

References

Chan, J. C. L. and W.M. Gray, 1982: Tropical cyclone movement and surrounding flow relationships. *Mon. Wea. Rev.*, 110, 1354–1374.

Chan, J. C. L., 2005: The physics of tropical cyclone motion. *Annu. Rev. Fluid Mech.*, 37, 99–128.

Emanuel, K. A., 1999: Thermodynamic control of hurricane intensity. *Nat.*, 401, 665-669.

Emanuel, K. A., 2003: Tropical cyclones. *Annu. Rev. Earth Planet. Sci.*, 31, 75-104.

Elsberry, R. L., W. M. Frank, G. J. Holland, J. D. Jarrell, and R. L. Southern. 1987: A global view of tropical cyclones, *Univ. Chicago Press*, 185 pp.

Erb, M. P., 2006: A case study of hurricane Katrina: rapid intensification in the Gulf of Mexico. *Proceedings of the National Conference on Undergraduate Research (NCUR) 2006, The University of North Carolina at Asheville, Asheville, North Carolina, April 6 – 8, 2006.*

Gray, W. M., 1968: Global view of the origin of tropical disturbances and storms. *Mon. Wea. Rev.,* 96, 669-700.

Gupta, A., R. K. Bansal, 1997: Performance of a global spectral model in predicting the track of a hurricane in the Bay of Bengal using synoptic vortex. *NCMRWF, New Delhi Tech. report*.

India Meteorological Department: 1996, Addendum to Storm Atlas from 1971 to 1990.

Kaplan, J., and M. Demaria, 2003: Large-scale Characteristics of Rapidly Intensifying Tropical Cyclones in the North Atlantic Basin. *Wea. Forecast*, 18, 1093-1108.

Kikuchi, K., B. Wang, and H. Fudeyasu, 2009: Genesis of tropical cyclone Nargis revealed by multiple satellite observations. *Geophys. Res. Lett*., 36, L06811, doi:10.1029/2009GL037296, 2009.

Li, C. Y., W. Zhou, J C L Chan, P Huang, 2011: Asymmetric modulation of the Western North Pacific cyclogenesis by the Madden-Julian Oscillation under ENSO conditions. *International Journal of Climatology* (in press)

Lin, I.- I., C.- H. Chen, I.- F. Pun, W. T. Liu, and C.-C. Wu, 2009: Warm ocean anomaly, air sea fluxes, and the rapid intensifi cation of tropical cyclone Nargis (2008). *Geophys. Res. Lett.*, 36, L03817, doi:10.1029/2008GL035815,

2009.

Liu, Q.Y., W. Zhou, 2010: The relationship between the northwestern Pacific typhoon activity and the upper-ocean heat content at interdecadal time scale. *J. Trop. Oceano*., 6, 4-8. (in Chinese).

Liu, Y.B, D.L. Zhang, and M.K.Yau, 1998: A Multiscale Numerical study of Hurricane Andrew (1992). Part II: Kinematics and Inner-Core Structures. *Mon. Wea. Rev.*, 127, 2597-2616.

Mandal, M., U.C. Mohanty, P. Sinha, M.M.Ali, 2007: Impact of sea surface temperature in modulating movement and intensity of tropical cyclones. *Nat. Hazards*, 41, 413-427.

McPhaden, M. J., G. R. Foltz, T. Lee, V. S. N. Murty, M. Ravichandran, G. A. Vecchi, J. Vialard, J. D. Wiggert, and L. Yu, 2009: Ocean-Atmosphere Interactions During Cyclone Nargis. *EOS*, 90(7), 53-60.

Mohanty, U.C., 1994: Tropical cyclones in the Bay of Bengal and deterministic methods for prediction of their trajectories. *Sadhana*, 19, 567-582.

Mohanty, U.C. and A. Gupta, 1997: Deterministic methods for prediction of tropical cyclone tracks. *Mausam*, 48, 257-272.

Orlanski, I., 1998: Poleward deflection of storm tracks, *J. Atmos. Sci.*, 55, 2577–2602.

Perrot, Pierre, 1998: A to Z of Thermodynamics. *Oxford University Press*, 336.

Prasad, K. and Y. V. Rama Rao, 2003: Cyclone Track prediction by a quasi-Lagrangian model. *Meteor. Atmos. Phys.*, 83,173-185.

Rao, K. AVR, 1997: Tropical cyclones–synoptic methods of forecasting. *Mausam*, 48,

239–256.

Shen, B.-W., W.-K. Tao, W. K. Lau and R. Atlas, 2010: Predicting tropical cyclogenesis with a global mesoscale model: Hierarchical multiscale interactions during the formation of tropical cyclone Nargis (2008). *J. Geophys. Res*., 115, D14102, doi:10.1029/2009JD013140, 2010.

Simpson, G., 1921: The southwest monsoon. *Quart. J. Roy. Meteor. Soc.*, 47(199), 155-172.

Velden, C. S. and L. M. Leslie. 1991: The basic relationship between tropical cyclone intensity and the depth of the environmental steering layer in the Australian region. *Wea. Forecast.* 6, 244-253.

Weber, H. C., 2001: Hurricane Track Prediction with a New Barotropic Model. *Mon. Wea. Rev.*, 129, 1834-1858.

Webster, P. J., 2008: Myanmar's deadly "daffodil". *Nat. Geosci.*, 1, 488-490.

Yanase, W., H. Taniguchi, and M. Satoh: 2010: The genesis of tropical cyclone Nargis (2008): environmental modulation and numerical predictability. *J. Meteor. Soc. Japan,* 88, 497-519.

Yamada, H., Q. Moteki, and M. Yoshizaki, 2010: The unusual track and rapid intensification of cyclone Nargis in 2008 under a characteristic environmental flow over the Bay of Bengal. *J. Meteor. Soc. Japan*, 88, 437-453.

Yokoi, S., and Y. N. Takayabu, 2010: Environmental and external factors in the genesis of tropical cyclone Nargis in April 2008 over the Bay of Bengal. *J. Meteor. Soc. Japan*, 88, 425-435.

Yuan, J. N., W. Zhou, H. J. Huang, F. Liao, 2009: Observational analysis of asymmetric distribution of convection associated with tropical cyclone "CHANCHU" and "PRAPIROON" making landfall along the south china coast. *J. Trop. Meteor.*, 25, 101-109.

Table and Figure Captions:

Table 1. TC genesis and landfall in the BOB during 1977–2008 (from JTWC). Three types of TC tracks are classified: eastward, northward, and westward.

Table 2. Chosen physical schemes and other simulation settings.

Fig. 1. TC landfalls in the BOB from 1977 to 2008 (JTWC record). Red, yellow, green solid lines indicate northward, westward, eastward track, respectively. Black solid dots represent the initial position of every TC.

Fig. 2. (a) The multilevel mass-weighted integral wind field (vector) and the corresponding U-wind field (shaded) of TC Nargis after recurvature (29 April); (b) The multilevel mass-weighted integral wind anomalies (vector) and the corresponding U-wind anomalies (shaded) of TC Nargis after recurvature (29 April), based on climatology from 1977–2008. Green solid dots indicate the pre-recurvature track of TC Nargis, and the orange solid dots refer to post-recurvature track of TC Nargis. Data are from NCEP/NCAR reanalysis.

Fig. 3. Wind fields at 500 hPa from 25 April to 02 May (i.e., throughout TC Nargis). Thick black arrows represent the significant wind pattern. Circles indicate southward cold air areas. "A" marks the anticyclonic circulation system. Data are from NCEP/NCAR reanalysis.

Fig. 4. Geopotential height anomoalies (shaded) and wind anomalies (vector) at 500 hPa after TC Nargis' recurvature (from 29 April to 2 May). "H" represents the high pressure system. Data are from NCEP/NCAR reanalysis.

Fig. 5. Vertical time section of cross-equatorial flow from 23 April to 2 May (throughout TC Nargis). The averaged region is (2.5°S–2.5°N, 70–80°E) marked by small rectangular in Fig. 3. The wind profile is shown by hatch marks; the meridional component of wind (U-wind) is in shaded. Data are from NCEP/NCAR reanalysis.

Fig. 6. Time series of TC Nargis intensity (from JTWC) using the lowest pressure in 6 h (hPa). Time series of area mean mid-level relative humidity (RH average on 700 hPa, 750 hPa, 800 hPa, and 850 hPa), from 18Z, 30 April to 18Z, 2 May (6-h intervals). Solid line and dash line indicate the region around TC Nargis and the selected southern area, respectively. Data are from NCEP/FNL dataset.

Fig. 7. Vertically integrated water vapor flux from surface to 300 hPa (vector, kg m^{-1} s^{-1}) and the amount of water vapor transport (shaded, kg m^{-1} s^{-1}) accumulated over (a) 29–30 April (as pre-RI period) and (b) 01–02 May (as RI period). Green solid dots indicate the track of TC Nargis, and the red solid dots emphasize the RI period. Data are from NCEP/NCAR reanalysis.

Fig. 8. Accumulated latent heat flux of (a1) pre-RI (29–30 April) and (a2) during RI (01–02 May). (b) Accumulated latent heat flux difference between (a) and (b) (b minus a). Green solid dots indicate the track of TC Nargis, and the red solid dots emphasize the RI period. Data are from the OAFlux dataset.

Fig. 9. Domain configuration for WRFV3 simulations (the rectangular indicates the region that TC Nargis was mainly affected by CEF-induced westerly wind).

Fig. 10. The observed (black solid line) and simulated tracks (blue solid line) of TC Nargis from 1200 UTC 27 April to 1800 UTC 02 May.

Fig. 11. Simulated wind fields at Eta-7 (around 850 hPa) and Eta-12 (around 500 hPa) levels from 1200 UTC 28 April to 1200 UTC 02 May with a 48-h time interval.

Fig. 12. (Left) Simulated relative humidity (in shaded) and wind fields (hatched) by control experiment; (right) relative humidity difference (in shaded) between

control and sensitive experiments with wind speed decreased by 50% and wind field of control experiment (hatched). All of them are at Eta-7 level (around 850 hPa) from 1200 UTC 28 April to 1200 UTC 02 May with a 48-h time interval.

Fig. 13. The observed (black solid dots) and simulated tracks (black solid stars) of TC Nargis from 1200 UTC 27 April to 1800 UTC 02 May, (a) with wind decreased by 50% at all levels; (b) with relative humidity decreased by 50% at all levels.

Fig. 14. Minimum central pressure of TC Nargis by control simulation (solid line) and numerical sensitivity simulation (dashed line) (a) with winds at all level decreased by 50%; (b) with relative humidity at all levels decreased by 50%.

Fig. 15. Schematic of the controlling factors on TC Nargis' track and RI.

Fig. 16. Tropical westerly jet evolution after TC Nargis' recurvature (from 29 April to 01 May). Zonal wind at 300 hPa is shaded.

.

Table 1 TC genesis and landfall in the BOB during 1977–2008 (from JTWC). Three types of track are classified: eastward, northward, and westward.

	Eastward	**Northward**	**Westward**	**Total**
Number	8	51	41	100
Mainly	Late Apr.	All	Oct.	
Occur	May	Month	Nov.	
Month			Dec.	
Percentage	8%	41%	51%	100%

Table 2. Chosen physical schemes and other simulation settings.

Options	**Simulation settings**
Simulation time	From 1200 UTC 27 April to 1800 UTC 02 May (total: 126 h)
Center of simulation region	95.0°E, 15.0°N
Horizontal resolution	30 km
Grid number of simulation	142*114, without nesting
Microphysics scheme	WSM 3 scheme
Radiation Scheme	RRTM scheme
Surface Scheme	Monin-Obukhov scheme
Planetary boundary layer	YSU scheme
Cumulus Convective scheme	Grell-Devenyi scheme
Input file	NCEP/FNL(1° × 1°)
Time step	60 s
Number of vertical levels	28 Eta_levels

Map projections	Mercator

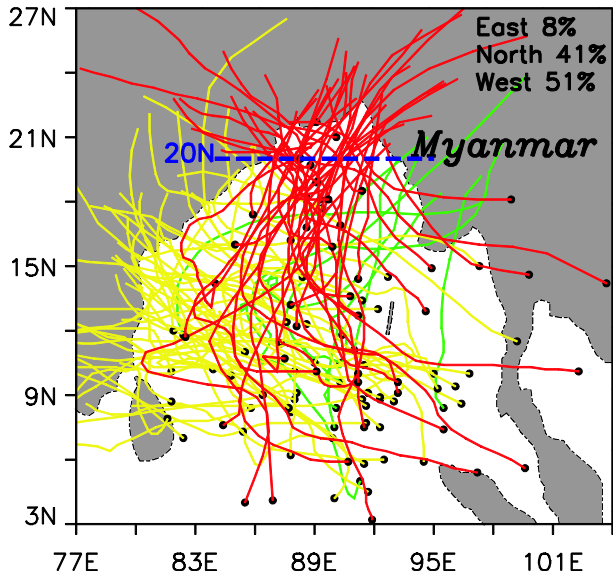

CORRECTIONS HAVE NOT BEEN MADE IN THESE DUPLICATED FIGURE CAPTIONS. SEE TEXT ABOVE FOR EDITS. COPY EDITOR

Fig. 1 TCs landfalling in BOB from 1977 to 2008 (JTWC record). Red, yellow, green solid line indicates northward, westward, eastward track, respectively. Black solid dots represent the initial position of every TC.

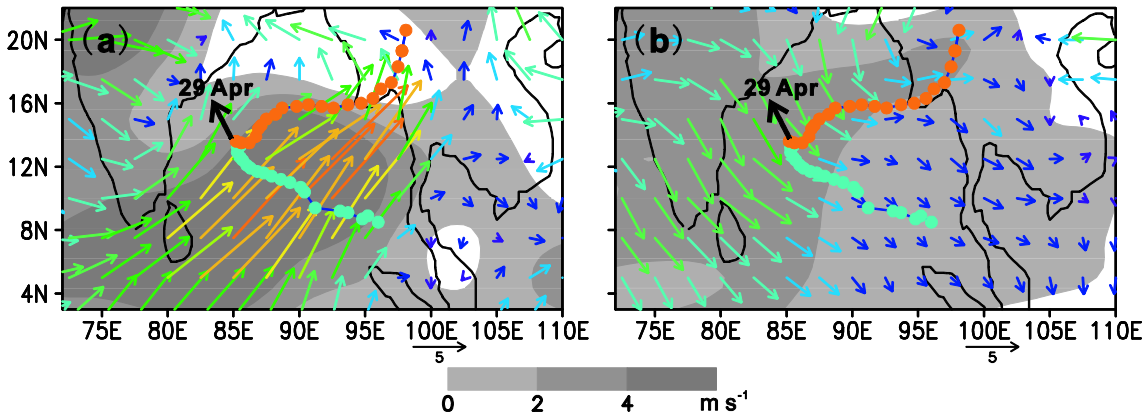

Fig. 2 (a) The multi-level mass-weighted integral wind field (vector) and the corresponding U-wind field (shaded) of Nargis after recurvature (29 April); (b) The multi-level mass-weighted integral wind anomalies (vector) and the corresponding U-wind anomalies (shaded) of Nargis after recurvature (29 April), based on climatology from 1977-2008. Green solid dots indicate the pre-recurvature track of Nargis, and the orange solid dots refer to post-recurvature track of Nargis. Data is

from NCEP/NCAR reanalysis.

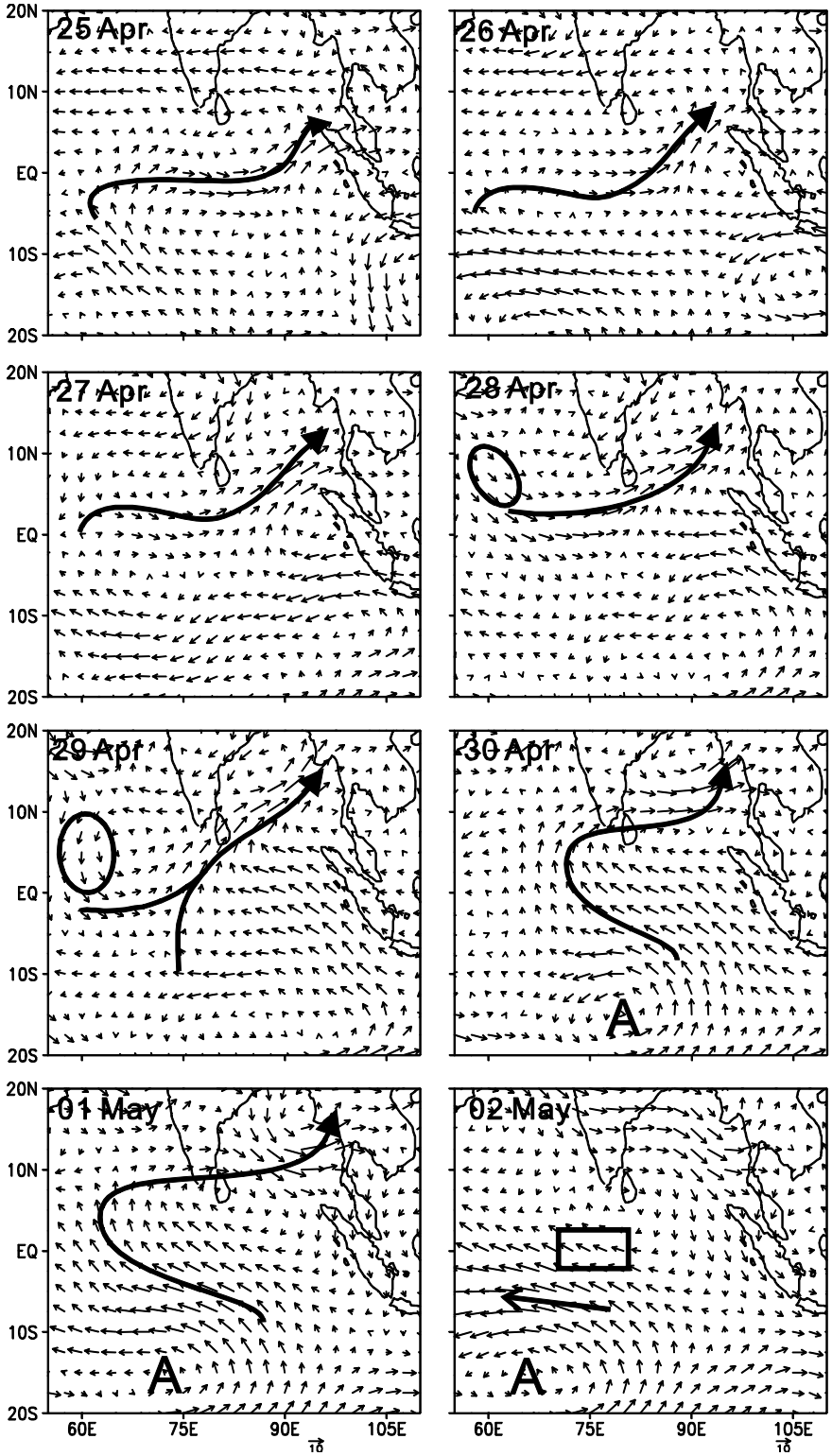

Fig. 3 Wind fields at 500hPa from 25 April to 2 May (throughout most lifecycle of Nargis). Thick black arrows represent the significant wind pattern. Circles indicate southward cold air areas. "A" marks the anticyclonic circulation system. Data is from

NCEP/NCAR reanalysis.

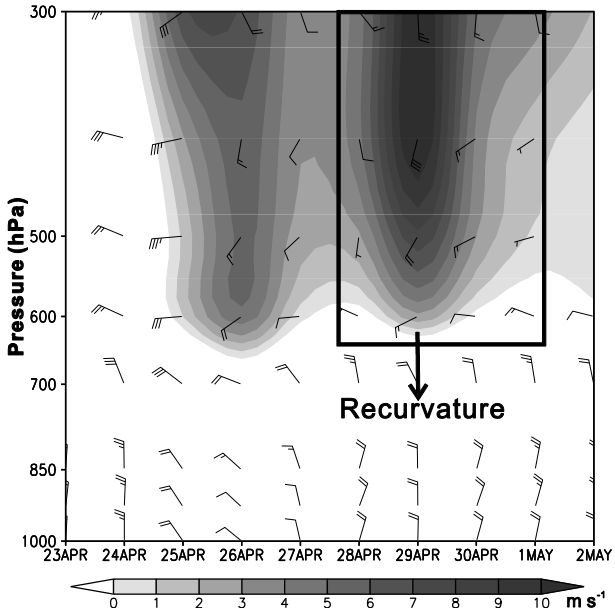

Fig. 4 Vertical time section of cross-equatorial flow from 23 April to 2 May (throughout lifecycle of Nargis). The averaged region is (2.5°S-2.5°N, 70°E-80°E) marked by small rectangular in Fig. 3. The wind profile is in barb, the meridional component of wind (V-wind) is in shaded. Data is from NCEP/NCAR reanalysis.

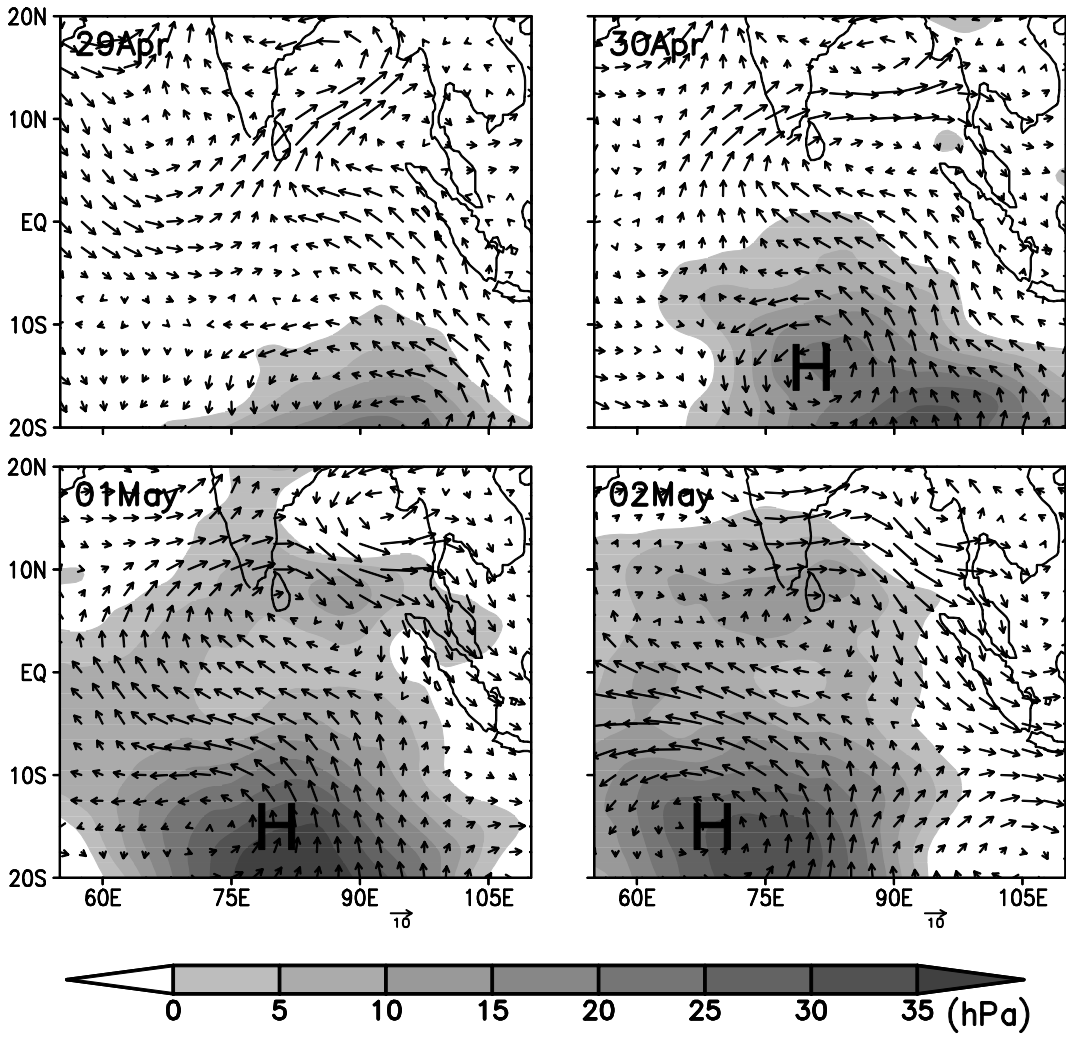

Fig. 5 Geopotential height anomoalies (shaded) and wind anomalies (vector) at 500hPa after Nargis' recurvature (from 29 April to 2 May). "H" represents the high pressure system. Data is from NCEP/NCAR reanalysis.

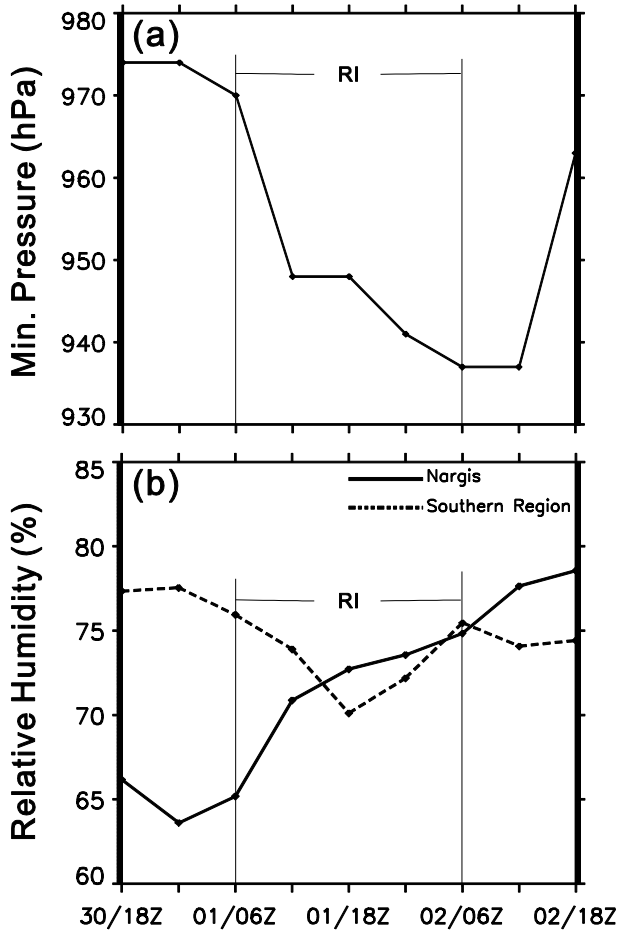

Fig. 6 Time series of Nargis intensity (from JTWC) using the lowest pressure in 6 h (hPa). Time series of area mean mid-level relative humidity (RH average on 700hPa, 750hPa, 800hPa, and 850hPa), from 18Z, 30 April to 18Z, 2 May (4 times a day). Solid line and dash line indicate the region around Nargis and the selected southern area, respectively. Data is from NCEP/FNL dataset.

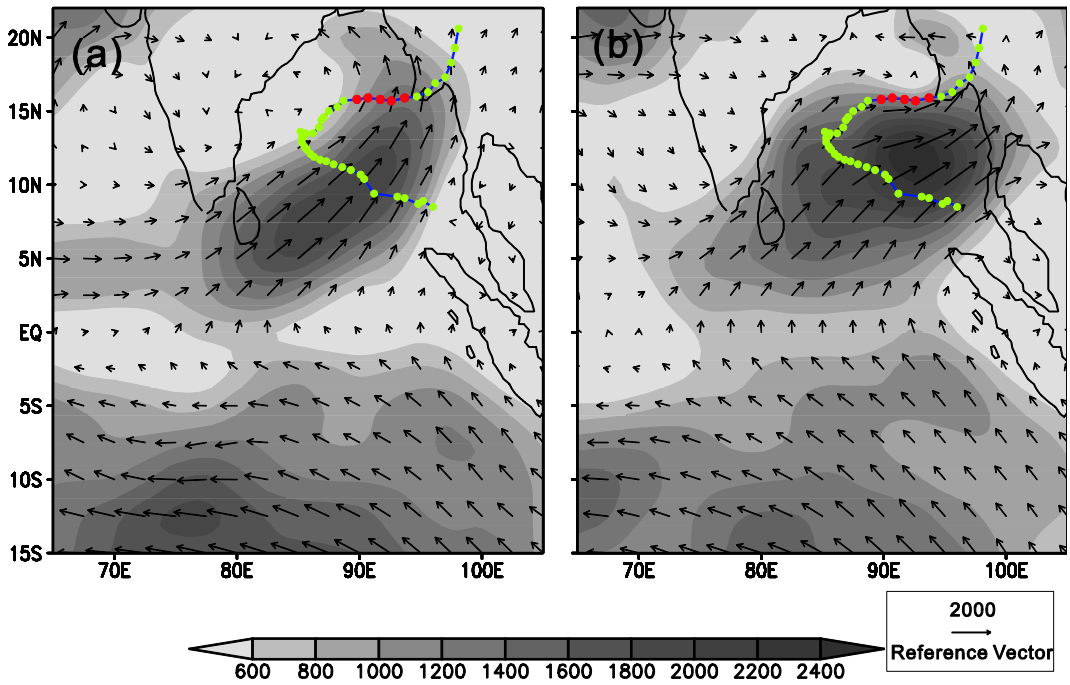

Fig. 7 Vertically integrated water vapor flux from surface to 300 hPa (vector, kg m^{-1} s^{-1}) and the amount of water vapor transport (shaded, kg m^{-1} s^{-1}) accumulated over (a) 29-30 April (as pre-RI period) and (b) 1-2 May (as during-RI period). Green solid dots indicate the track of Nargis, and the red solid dots emphasize the RI period. Data is from NCEP/NCAR reanalysis.

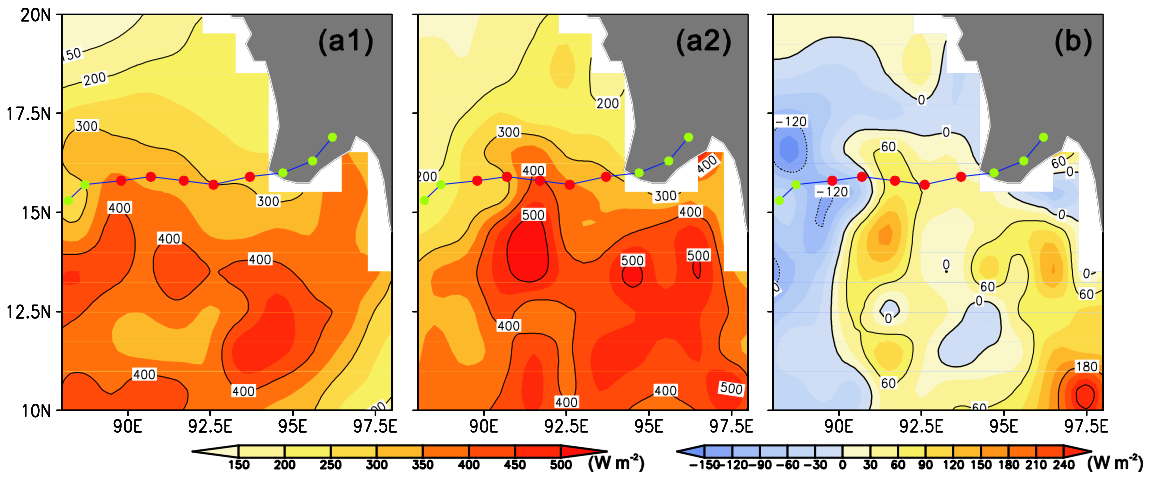

Fig. 8 Accumulated latent heat fluxof (a1) pre-RI (29-30 April) and (a2) during RI (1-2 May). (b) Accumulated latent heat flux difference between (a) and (b) (b minus a). Green solid dots indicate the track of Nargis, and the red solid dots emphasize the RI period. Data is from OAFlux dataset.

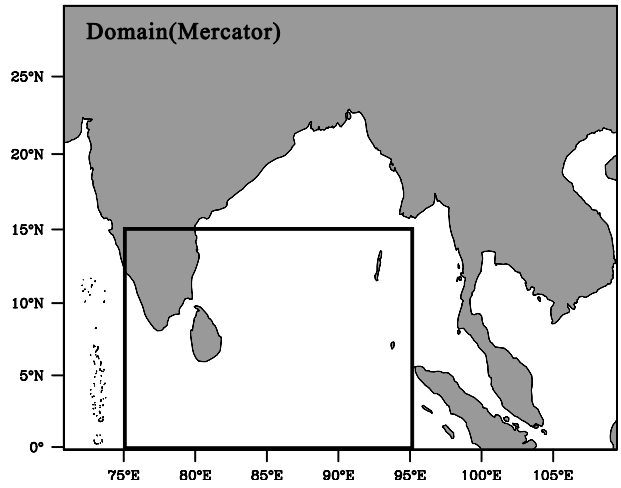

Fig. 9 Domain configuration for WRFV3 simulations (the rectangular indicates the region that Nargis mainly affected by CEF-induced west wind).

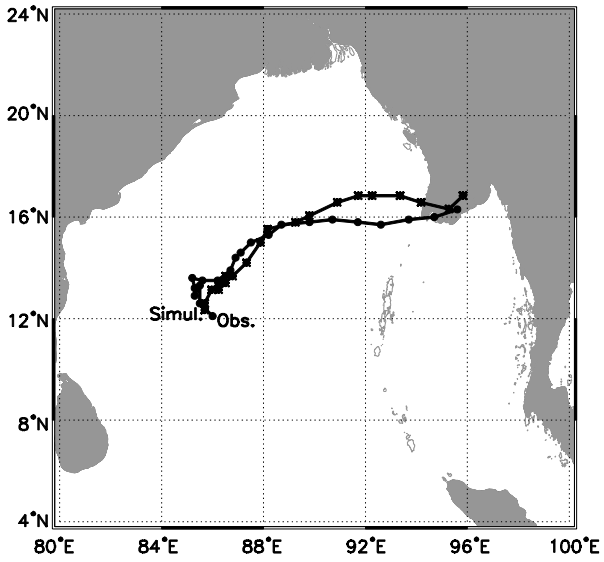

Fig. 10 The observed (black solid dots) and simulated tracks (black solid stars) of Nargis from 1200 UTC 27 April to 1800 UTC 02 May.

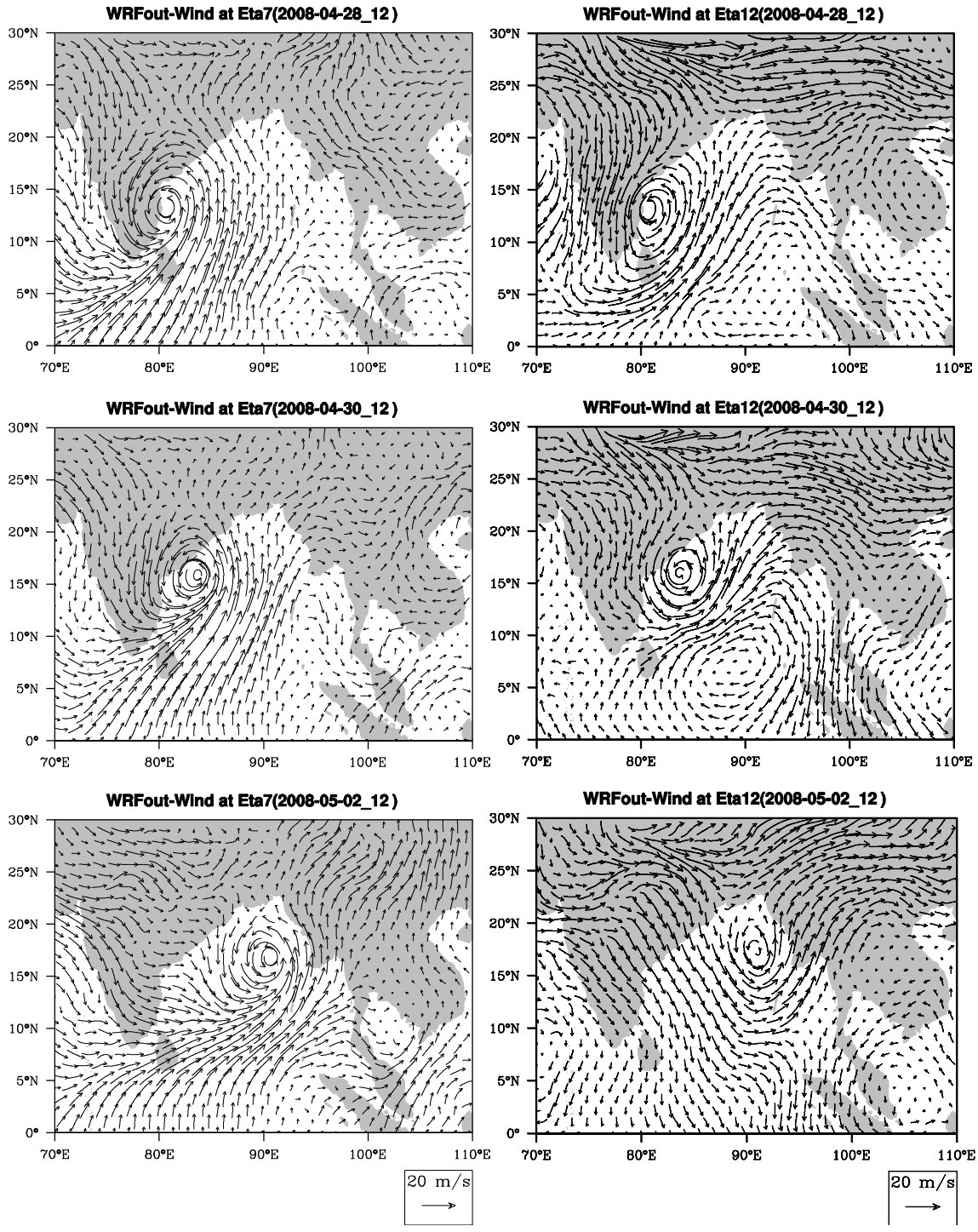

Fig. 11 Simulated wind fields at Eta-7 (around 850hPa) and Eta-12 (around 500hPa) levels from 1200 UTC 28 April to 1200 UTC 02 May with 48h time interval.

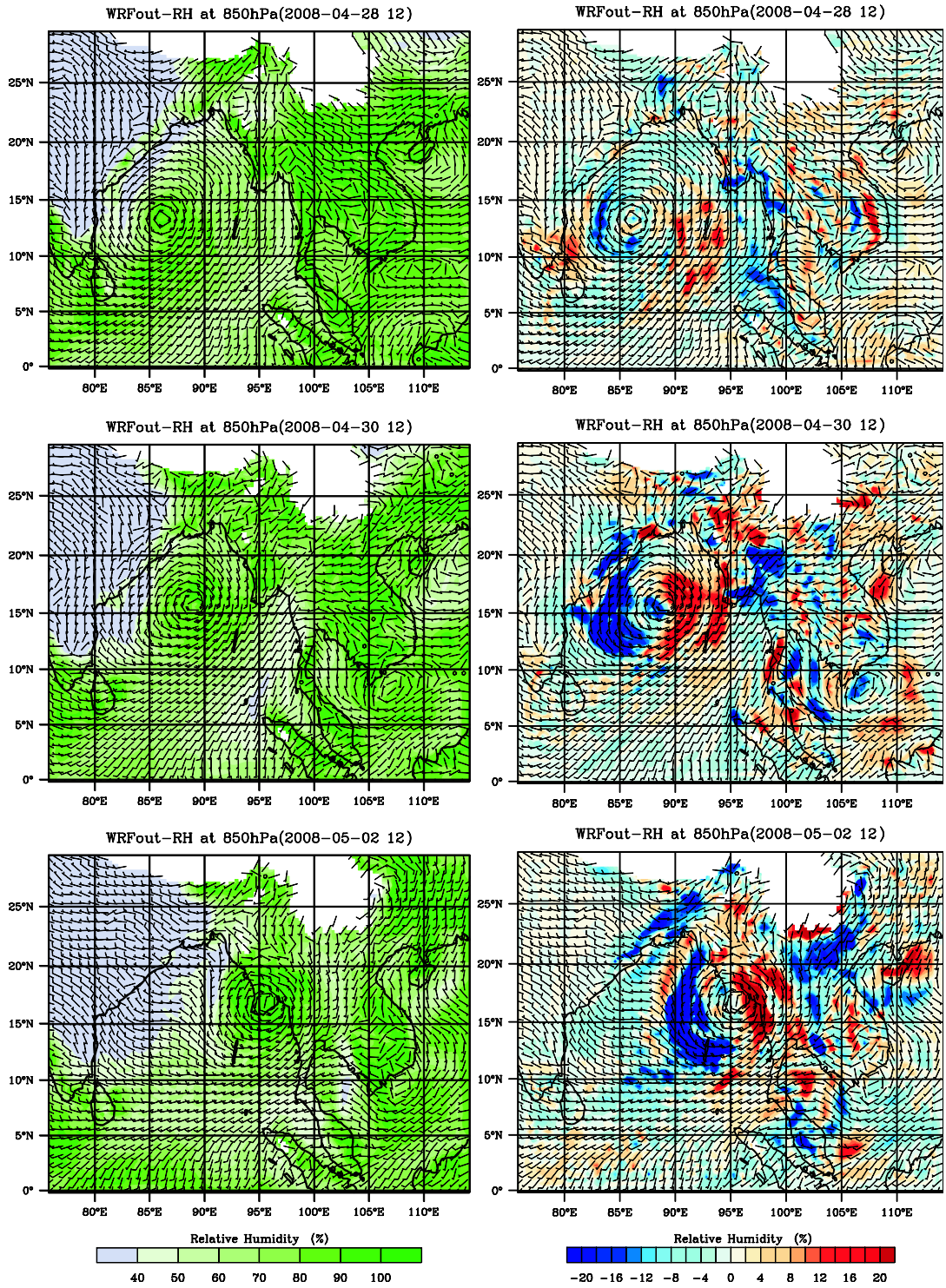

Fig. 12 The left panel: simulated relative humidity (in shaded) and wind fields (in barb) by control experiment; right panel: relative humidity difference (in shaded) between control and sensitive experiments with wind speed decreased by 50% and wind field of control experiment (in barb). All of them are at Eta-7 level (around 850hPa) from 1200 UTC 28 April to 1200 UTC 02 May with 48h time interval.

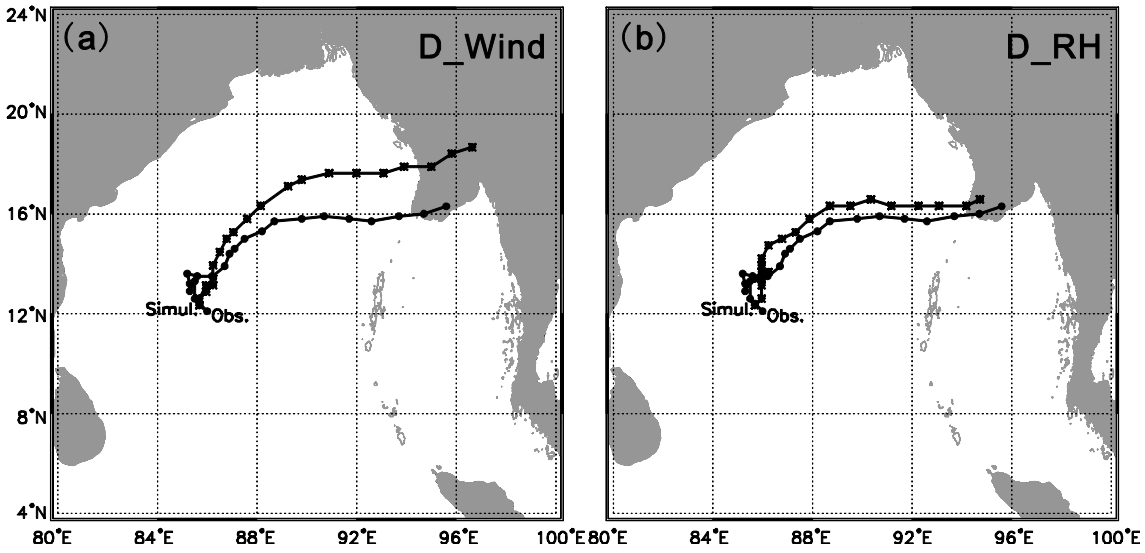

Fig. 13 The observed (black solid dots) and simulated tracks (black solid stars) of Nargis from 1200 UTC 27 April to 1800 UTC 02 May, (a) with wind decreased by 50% at all level; (b) with relative humidity decreased by 50% at all level.

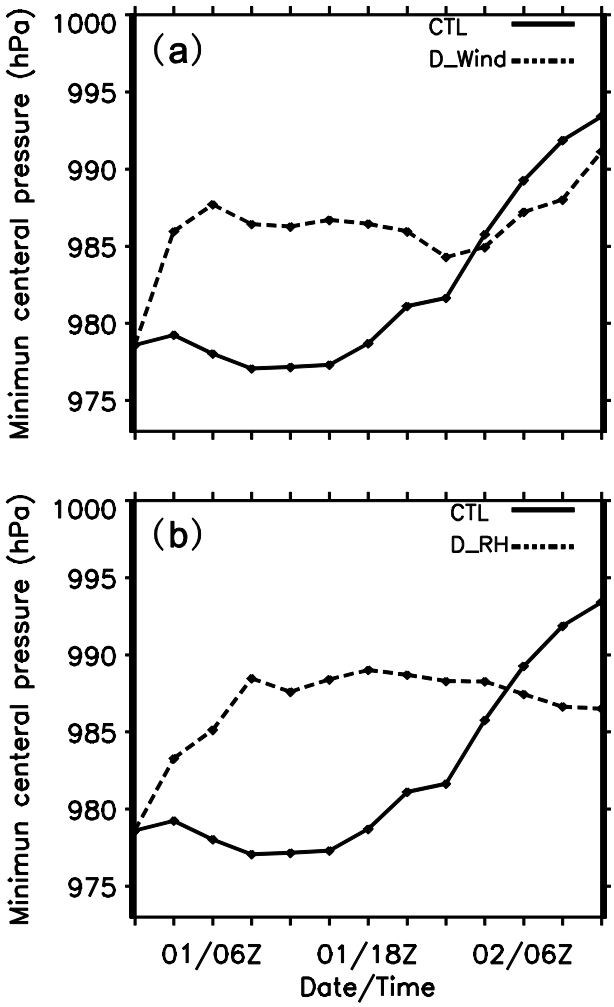

Fig. 14 Mininum central pressure of Nargis by control simulation (solid line) and numerical sensitivity simulation (dash line) (a) with wind at all level decreased by 50%; (b) with relative humidity at all level decreased by 50%.

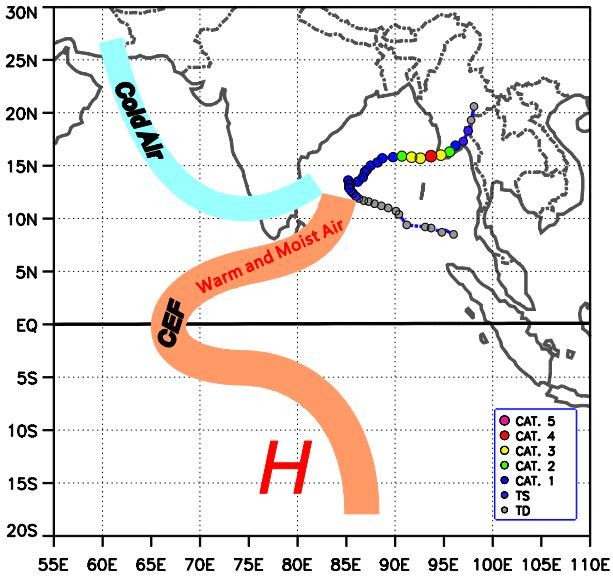

Fig. 15 Schematic of the controlling factors on Nargis' track and RI.

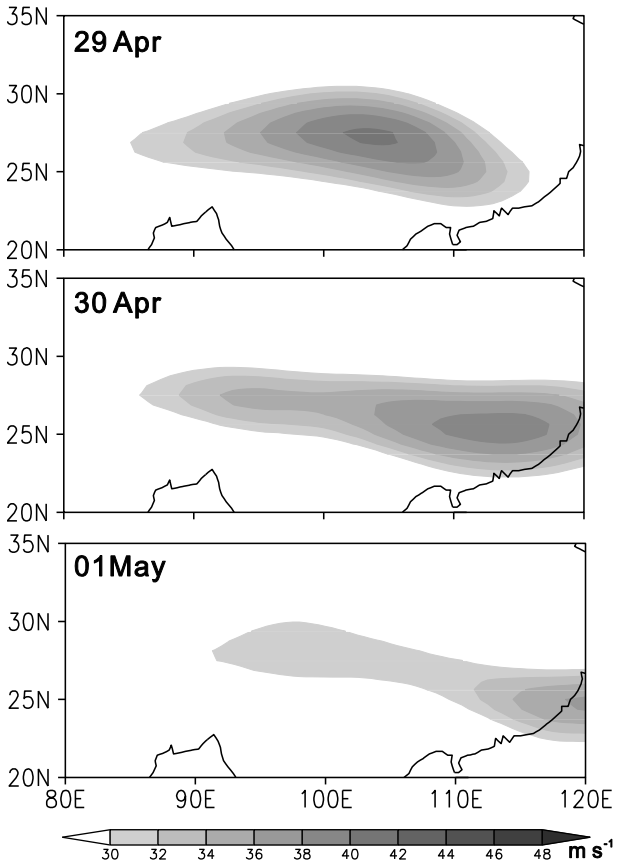

Fig. 16 Tropical westerly jet evolution after Nargis' recurvature (from 29 April to 1 May). Zonal Wind at 300hPa is in shaded.